J Mater Sci: Mater Electron (2021) 32:16682–16693

Room temperature deposition of pulsed laser-assisted (Al, In) co-doped ZnO transparent conducting films appropriate for flexible substrates

Santanu Pal[1], Shuvaraj Ghosh[1], and Durga Basak[1,*]

[1] *School of Physical Sciences, Indian Association for the Cultivation of Science, 2A and 2B Raja S. C. Mullick Road, Kolkata 700032, India*

Received: 30 January 2021
Accepted: 18 May 2021
Published online:
31 May 2021

ABSTRACT

Transparent conducting (TC) films based on Al and In co-doped ZnO (AIZO) are deposited at room temperature (RT) onto glass as well as flexible polyethylene terephthalate (PET) substrates by pulsed laser deposition (PLD) technique. While substrate heating becomes inevitable to obtain enough conductivity of the oxide films, we simply by controlling the chamber O_2 pressure (3×10^{-3} to 1.5×10^{-2} mbar) have achieved the desired structural, electrical and optical properties of the AIZO films without the need to heat the substrate. All the co-doped films having hexagonal wurtzite structure of ZnO shows surface roughness values in the range of 2.3–4.4 nm. The average transparency of the films is 79–92% in the 400–700 nm range. The film deposited at O_2 pressure of 3×10^{-3} mbar on glass substrate shows the highest carrier concentration value of 1.60×10^{21} cm^{-3} with the lowest sheet resistance of 30.47 Ω/sq as well as the lowest roughness value of 2.3 nm. The best condition used for the AIZO film deposited on PET substrate shows unprecedentedly low sheet resistance of only 32.63 Ω/sq which opens up enormous possibility for flexible electronics.

1 Introduction

Transparent conducting films (TCFs) are composed of a special type of material which has unique combination of high electrical conductivity and high optical transparency in the visible region of the solar spectrum. There are diverse applications of TCFs as transparent electrode in various optoelectronic devices such as flat panel displays (FPDs) [1–3], light-emitting diodes (LEDs) [4, 5], organic light-emitting diodes (OLEDs) [6, 7], solar cells [8–10], etc. Tin-doped indium oxide (ITO) and fluorine-doped tin oxide (FTO) are the two commercially used most popular TCFs because of their high electrical conductivity as well as high optical transparency [11–16]. However, these are costly and due to exhausting In source, In-rich ITO is expected to be lacking. The growing demand of TCFs in the optoelectronic

Address correspondence to E-mail: sspdb@iacs.res.in

https://doi.org/10.1007/s10854-021-06224-7

industry day by day has led to a quest for a low-cost TCF to decrease the fabrication cost of various electronic and optoelectronic devices. Nontoxic, abundant, inexpensive trivalent metal ion-doped ZnO thin film being an immensely promising substitute of ITO, a renewed interest has been focused on ZnO which had been a material of research in 1950s [17, 18]. Al-doped ZnO (AZO) thin films have now been widely and successfully used as TCFs in many optoelectronic devices [7, 19, 20]. However, ITO, FTO as well as AZO thin films show high optical transparency and conductivity only when a heat treatment of minimum 300 °C and above (either substrate or post-growth annealing temperature) is applied [21–24]. Ironically laying a TCF on flexible substrate with high conductivity and high visible-light transparency is inevitable to fabricate flexible electronic devices in the current age. Flexible substrates such as polyethylene terephthalate (PET), polyethylene naphthalate (PEN), poly carbonate (PC), etc., can withstand a maximum temperature of 180 °C which again is not high enough for the above-mentioned oxide TCFs to achieve enough quality to show the requisite properties [25]. The commercially available ITO-coated PET substrate shows a sheet resistance of 60 Ω/sq for a 130-nm-thick ITO film [26]. Most of the studies on trivalent cation-doped ZnO films show properties comparable to an ITO film involve either a high film deposition temperature or a post-deposition annealing at high temperature [27–32]. Therefore, development of room or low-temperature deposited ZnO-based TCFs on flexible substrate is highly required and timely enough.

Often for a single metal ion doping in ZnO, resistivity begins to increase beyond a certain dopant concentration, which is generally attributed to appearance of a separate oxide phase due to solubility limit of that particular dopant in ZnO. To overcome this limitation, scientists have attempted co-doping, i.e., use of a second metal cation together with another one [29, 33–37]. Cation–cation co-doping generally increases the solubility limit of the total dopants beyond the solubility limit of individual dopant [38].

Among various thin film deposition techniques, pulsed laser deposition (PLD) is relatively a flexible, promising, simplest, and widely exploited technique for the preparation of metal oxide and complex metal oxide films with a wide range of pressure ranging from atmospheric to few mTorr in any background gas environment [39, 40]. Therefore, in this work, we have grown Al (1 at.%) and In (1 at.%) co-doped ZnO thin films on glass substrates at room temperature (RT) using PLD technique. In this study, various excimer laser energies (180 to 400 mJ) incident on the target and oxygen (O_2) chamber pressures (3×10^{-3} to 1.5×10^{-2} mbar) have been chosen to control the optical transparency as well as conductivity of the films in order to optimize the best deposition conditions for the film on PET substrate. It has been seen that the lowest laser energy although produces a Al, In co-doped ZnO (AIZO) film with the highest sheet resistance, but the quality of the film is the best in terms of structural as well as optical transparency. The AIZO thin films on glass substrates deposited with 180 mJ laser power have an average transparency of 79–92% in the 400–700 nm wavelength region. The lowest resistivity value of 1.10×10^{-3} Ω.cm (sheet resistance 30.47 (Ω/sq) and the highest carrier concentration value of 1.60×10^{21} cm^{-3} have been achieved for the films deposited with 3×10^{-3} mbar O_2 pressure. Therefore, the lowest laser power, i.e., the best deposition conditions have been used to deposit AIZO film on PET substrate which shows a sheet resistance value of 32.63 Ω/sq which is quite less than that of commercially available ITO-coated PET substrate [26]. Evidently such a low sheet resistance is a benchmark since we have obtained this value using only 1 at.% In, while use of ITO film consumes 80% In by weight [41].

2 Experimental

AIZO target for PLD was prepared by conventional ceramic technique using high-purity commercial ZnO (> 99%, MERCK), Al_2O_3 (> 99.5%, MERCK) and In_2O_3 (99.99% Alfa Aesar) powders. To prepare the target 31.6 mg of Al_2O_3 and 86.1 mg of In_2O_3 were mixed with 5 g of ZnO powder (to achieve 1 at.% doping of each In and Al) thoroughly in an agate mortar-pestle for several hours, followed by a pressing under 5 ton pressure to form a pellet with a diameter of 1.5 cm. The pellet was then sintered in a tubular furnace at 850 °C for 24 h in ambient condition for a solid-state reaction.

After checking the phase purity of the target, it was used for thin film deposition using PLD. A coherent Kr-F excimer laser of emission wavelength 248 nm, with a repetition rate 6 Hz and energy 180 mJ, 300 mJ, 400 mJ were used to vaporize the sintered target. The AIZO films were also deposited using various background O_2 pressures ranging from 3×10^{-3} to 1.5×10^{-2} mbar respectively at RT at 180 mJ energy. The number of laser pulses used for each film deposition was 20,000. Before backfilling with different O_2 pressures, the vacuum chamber of the deposition system was evacuated to a base pressure of 4×10^{-6} mbar by rotary and turbo molecular pumps. For each deposition, a distance of 10 cm between the target and the substrate was kept fixed. The chamber O_2 pressure during a deposition was maintained by controlling the gas flow rate and turbo speed simultaneously. AIZO film at 3×10^{-3} mbar O_2 pressure and 180 mJ energy has also been deposited on a flexible PET substrate.

The phase purity and crystallinity of the thin films have been determined by X-ray diffractometry (XRD; BRUKER model: D8) using Cu Kα (λ = 1.5418 Å) radiation. The surface morphology has been investigated by the atomic force microscopy (AFM; Veeco; model diCP-II) and field-emission scanning electron microscopy (FESEM; JEOL; model: JSM-6700F). The thicknesses of the films were determined from the cross-sectional FESEM images. The transmittance properties of the films were measured using UV–VIS spectrophotometry (PerkinElmer, Lambda 35). To eliminate the effect of glass substrate an auto zero has been performed before taking the transmission spectra. Room temperature electrical parameters of the films were measured using a Hall Effect measurement system (HEMS, Nano Magnetic Instruments) in the four probe Van der Pauw geometry. Ohmic contacts of Al with thickness 90 nm were deposited on the top of the film using a thermal evaporation unit. X-ray photoelectron spectroscopy (XPS; Omicron, serial no: 0571) was studied to identify the chemical states of the elements using Al-Kα X-ray beam as the excitation source (1486.7 eV). The nomenclatures of the thin films deposited on glass and PET substrates at various laser energies and O_2 pressures have been noted in Table 1.

3 Results and discussion

Figure 1a shows the XRD patterns of the films deposited on glass substrates with various laser energies at 3×10^{-3} mbar O_2 pressure. The (002) peak (JCPDS card No. 36–1451) of hexagonal wurtzite structure is the prominent peak for all the films. The full width at half maximum (FWHM) value of the peaks decreases as the laser energy decreases. The crystallite size (D) as calculated using the Scherrer equation [42, 43]:

$$D = \frac{0.9\lambda}{\beta \cos\theta} \tag{1}$$

where λ is the wavelength of the incident X-ray, β is the FWHM of (002) peak, decreases as laser energy increases. This indicates improvement in the structural quality with decrease in laser energy. This may be due to the fact that at higher laser energy, the large chunk of ablated energetic particles hits the deposited layers on the substrate and degrades the crystallinity. The stress values (ϕ) for the films as listed in Table 2 are determined using the following formula [44]:

$$\phi = \frac{2c_{13}^2 - c_{33}(c_{11} + c_{12})}{2c_{13}} \times \frac{C - C_0}{C_0} \tag{2}$$

where C_{11} = 208.8 GPa, C_{12} = 114.7 GPa, C_{13} = 104.2 GPa, C_{33} = 213.8 GPa are the elastic constants. C and C_0 (5.206 Å) are the axis length of the strained and unstrained films. It has been observed that as the laser energy increases the stress value also increases. For the AIZO films, the calculated stress is compressive in nature. Figure 1b shows the transmission spectra of the AIZO films deposited at 3×10^{-3} mbar O_2 pressure at various laser energies. It has been observed that as the energy decreases average transmission in the visible range increases which may be due to a decrease in the film thickness with a decrease in laser energy. From the undulation in the transmission spectra it is also clear that thickness of the films increases as the laser energy increases. Table 2 summarizes the effect of laser energy on the structural and optical properties of the AIZO films at a fixed O_2 pressure (3×10^{-3} mbar).

As the quality of a TCF is determined by the value of figure of merit (FOM) values. The FOM value is calculated using Haacke formula as follows [30]:

$$FOM = \frac{T^{10}}{R_s} \tag{3}$$

where T is the average absolute transmission in the visible range and R_s is the sheet resistance value.

Table 2 shows that FOM value has been increased as the laser energy decreases. Moreover the films deposited at higher laser energies shows poor

Table 1 Nomenclature, laser energy, O_2 pressure and substrate type of the AIZO films

Sample name	Specifications		
	Laser energy (mJ)	O_2 pressure (mbar)	Substrate type
3G40	400	3×10^{-3}	Glass
3G30	300	3×10^{-3}	Glass
3G18	180	3×10^{-3}	Glass
6G18	180	6×10^{-3}	Glass
10G18	180	1.0×10^{-2}	Glass
15G18	180	1.5×10^{-2}	Glass
3P18	180	3×10^{-3}	PET

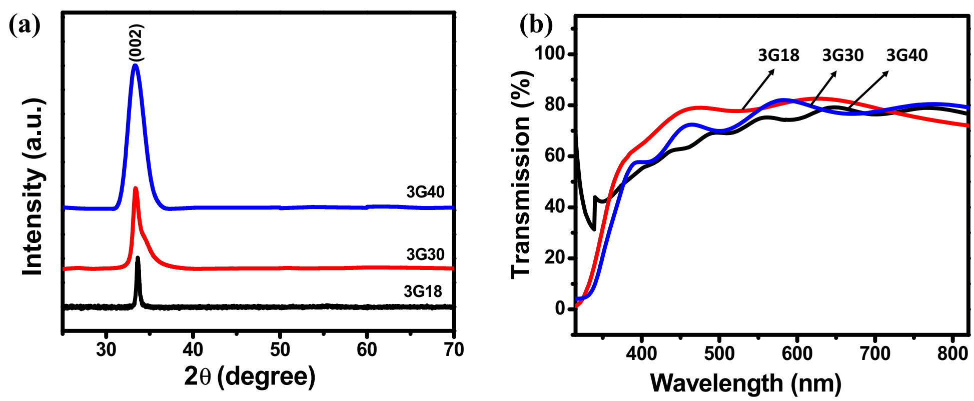

Fig. 1 **a** XRD pattern and **b** transmission spectra of the AIZO films deposited at various energies at 3×10^{-3} mbar O_2 pressure

Table 2 (002) peak position, FWHM values, crystallite size, *C*-axis length, compressive stress, average transmission in visible region, sheet resistance and FOM values of the various AIZO films deposited at various laser energies at 3×10^{-3} mbar O_2 pressure

Sample name	(002) peak position (degree)	FWHM (degree)	Crystallite size (nm)	C-axis length (Å)	Compressive stress (GPa)	Average transmission in visible region (%)	Sheet resistance (Ω/sq)	FOM ($\times 10^{-3}$) (Ω^{-1})
3G40	33.33	2.05	4.23	5.376	7.61	71.34	15.45	2.21
3G30	33.39	1.60	5.42	5.367	7.79	75.01	19.27	2.96
3G18	33.63	0.34	25.50	5.326	5.35	79.25	30.47	3.20

crystallinity as well as low average transmission in the visible range. Considering the criteria of maintaining good crystalline quality, high optical transmission and low sheet resistance, we have chosen 180 mJ laser energy to deposit films at various O_2 pressure to study further the effect of O_2 pressure in the AIZO films.

The XRD pattern of the films deposited with 180 mJ laser energy at various O_2 pressures as shown in Fig. 2a also shows the presence of a prominent (002) peak, the intensity of which decreases as the oxygen pressure increases. Also, the other peaks (100) and (101) appear as the oxygen pressure increases. No phase corresponding to other oxides was detected implying perfect incorporation of Al and In dopants in ZnO lattice.

From Fig. 2a, it has been observed that the orientation of the films depends on the deposition pressure. Weaker intensity of (002) peak and appearance of the (100) and (101) peaks in the 10G18 and the 15G18 films suggest random growth of the crystallites are invigorated. Further, a degradation in the crystalline quality is also evident from the FWHM values of the (002) peak as shown in Table 3. The crystallite size (D) as calculated using the Scherrer equation decreases as O_2 pressure increases. The stress values for the films as listed in Table 3. The crystallization of thin films depends on the kinetic

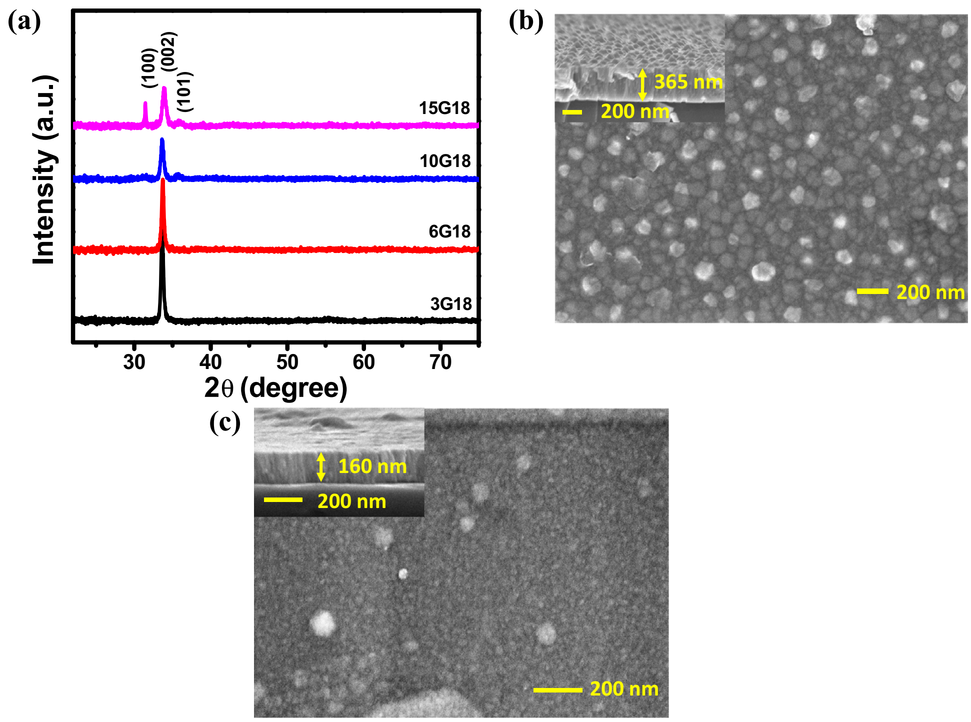

Fig. 2 **a** XRD pattern of the AIZO films deposited at various O_2 pressure. **b** Top-view FESEM image of the 3G18 and **c** 15G18 film. The inset shows the cross-section view of the corresponding films

energy of the atoms present in the plasma plume of the ablated target material. At lower O_2 pressure the atoms present in the plasma plume have sufficient kinetic energy to find the lowest energy sites by surface diffusion. When the pressure is higher the collision probability of the atoms vaporized from the target with the ambient O_2 molecules become higher, thereby the atoms reach the substrate after losing a part of their kinetic energy via several collisions preventing the possibility of the adatoms to look for the thermodynamically stable position. As a result, these ablated target atoms sit at random sites as available which caused random growth orientation and low crystallinity [45, 46].

The surface morphology as shown in top-view FESEM image (Fig. 2b) of the 3G18 film reveals granular texture. The cross-section view shows a growth of a 365 nm thick film. The homogeneous grain growth is evident from the top-view image. The cross-section view also shows a very compact film nature. Figure 2c shows smaller grain size for the 15G18 film, and from the inset it is evident that film thickness decreases with an increase in the O_2 pressure. This may be due to the fact that the collision of the O_2 gas molecules with the ablated materials decreases the film deposition rate.

The 3D topological images obtained from the AFM studies for the films deposited at 180 mJ energy at various O_2 pressure are shown in Fig. 3. The root mean square (RMS) roughness values as calculated by WSxM 4.0 software are listed in Table 3.

Table 3 (002) peak position, FWHM values, crystallite size, C-axis length, compressive stress and RMS roughness of the various AIZO films deposited at energy of 180 mJ

Sample name	(002) peak position (degree)	FWHM (degree)	Crystallite size (nm)	*C*-axis length (Å)	Compressive stress (GPa)	RMS roughness(nm)
3G18	33.63	0.34	25.50	5.326	5.35	2.3
6G18	33.71	0.35	24.78	5.313	4.77	2.4
10G18	33.63	0.46	18.85	5.326	5.35	2.3
15G18	33.85	0.54	16.07	5.292	3.84	4.4

It has been observed that with an increasing O_2 pressure from 3×10^{-3} to 1.5×10^{-2} mbar, the RMS roughness is increased from 2.3 to 4.4 nm as shown in Table 3.

The XPS wide survey spectra of the films as shown in Fig. 4a shows the presence of Zn, O and In. Prior to taking each scan, the film surface was sputtered for 300 s by Ar ion to clean the surface. Figure 4b shows that the In 3d spectrum has been split into two peaks ($3d_{3/2}$ and $3d_{5/2}$). A weak Al $2p_{3/2}$ is also observed as shown in Fig. 4c, which confirms the co-doping of Al and In into ZnO. The peak signal of Al can only be detected in the slow scan spectra probably owing to a small value of ionization cross-section [47]. Figure 4d shows the doublet splitting of the Zn 2p peak. Figure 4e and f shows the XPS spectra of the O 1 s peak of the 3G18 and 15G18 films respectively. Because of an asymmetric nature in the higher binding energy side of both the O 1 s peaks, the peaks have been well-fitted with two Gaussian peaks. The fitted peak (P1) having higher intensity is centered around 530.70 eV which is attributed to the O^{2-} ions in the ZnO wurtzite lattice structure, i.e., lattice oxygen. However, the fitted peak (P2) with lower intensity centering around 531.6 eV corresponds to O^{2-} ions in the oxygen deficient regions, i.e., oxygen vacancy (V_O) in ZnO lattice [41]. The embedded table in Fig. 4 indicates the decrease in V_O defects with an increase in the O_2 pressure which may be due to more oxygen incorporation into the ZnO lattice. From the XPS spectra we have calculated the percentage of concentration of the various elements as listed in Table 4 which also proves that with an increase in O_2 pressure more oxygen is incorporated into the films.

The UV–VIS transmission spectra of the AIZO films as presented in Fig. 5a show a very high transparency in the visible region with the transmission value of 79–92% in the wavelength range 400–700 nm for films deposited at 180 mJ energy. The inset in Fig. 5a shows the digital image of the clearly visible write-up "IACS" underneath the AIZO-coated glass substrate which proves the transparency of the films. It has been observed that the average transparency increases with O_2 pressure which is quite normal. A sharp band-edge absorption below 400 nm has been observed with a shifting of the band-edge absorption to a higher wavelength side for the films deposited at higher O_2 pressures. The bandgap for each film has been calculated using Tauc plot ($(\alpha h\nu)^2$ vs $h\nu$) [48]. The bandgap increases as the O_2 pressure decreases as shown in the table in Fig. 5b which can be explained by the Burstein–Moss effect [49–51].

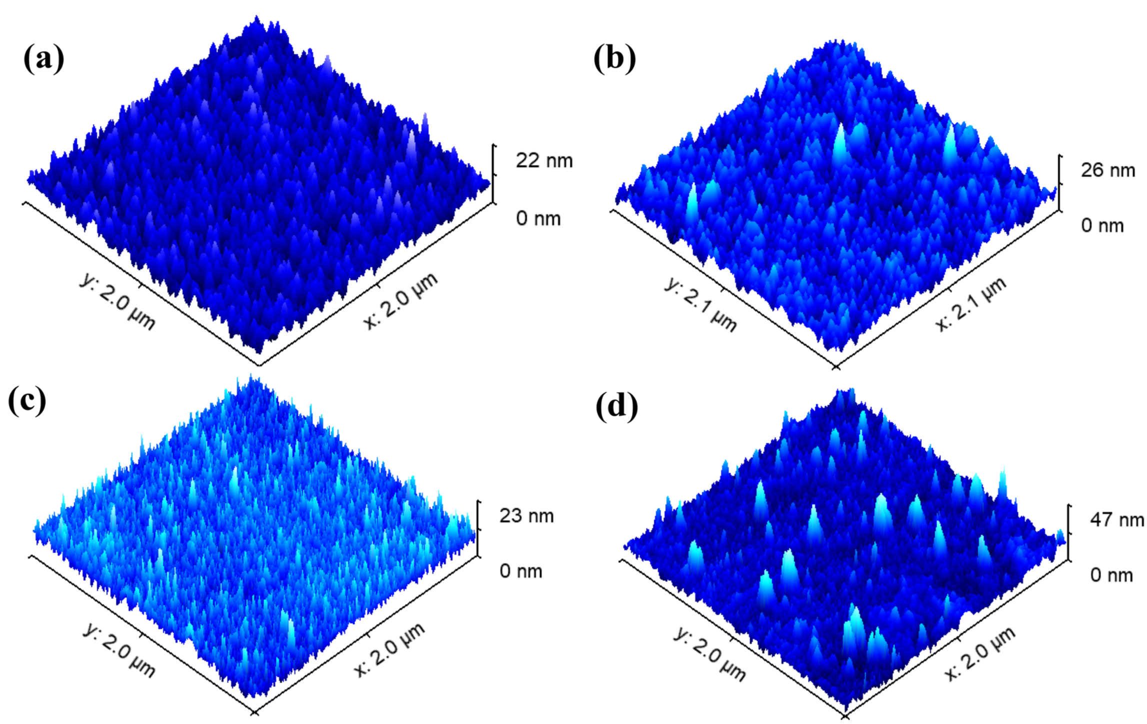

Fig. 3 AFM images of the **a** 3G18, **b** 6G18, **c** 10G18, and (d) 15G18 films

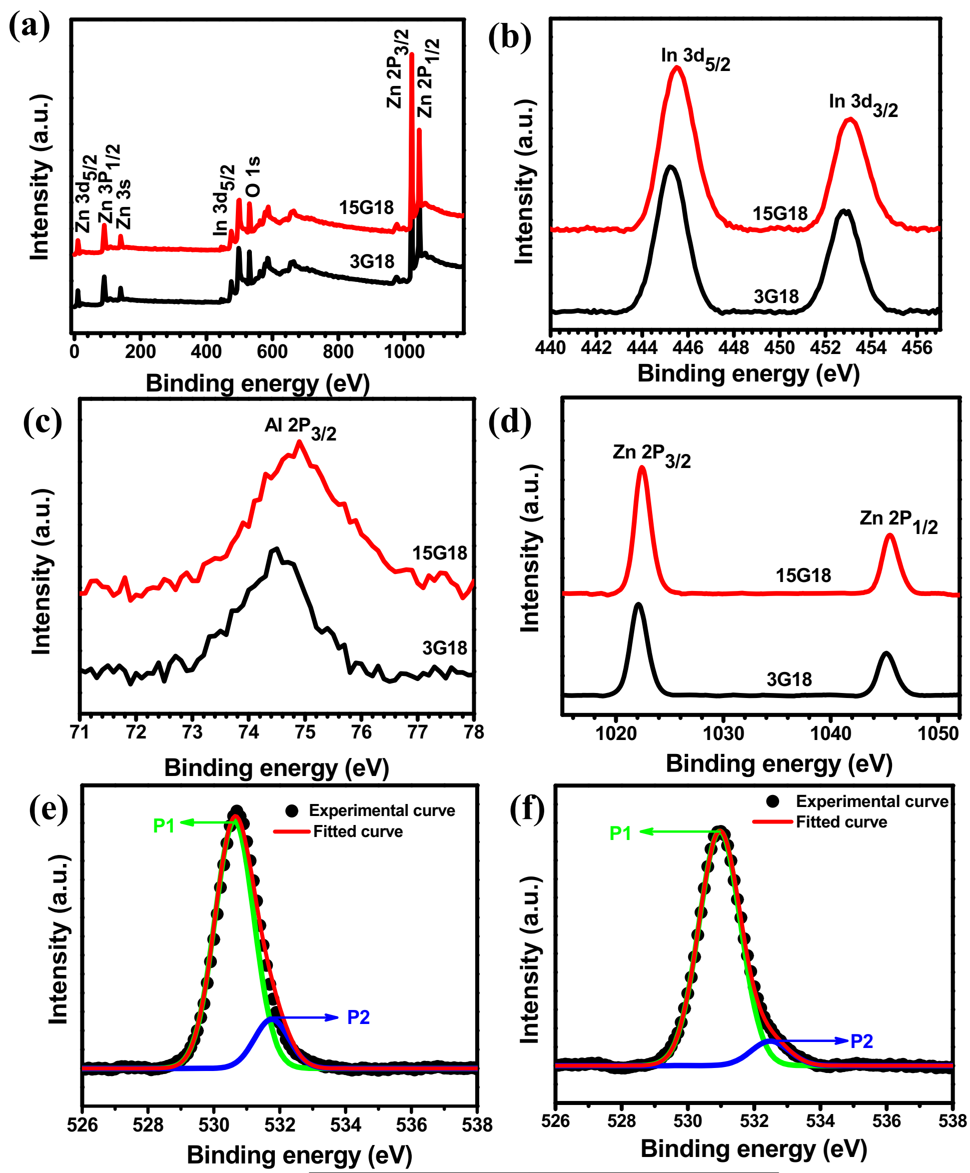

Sample name	V_O/(Lattice O + V_O)
3G18	14.89%
15G18	8.68%

Fig. 4 **a** XPS full scan spectra, **b** In 3d peak, **c** Al 2p peak **d** Zn 2p peak of the 3G18 and 15G18 films. Gaussian de-convolution of O 1 s peak and percentage of V_O (P2) with respect to lattice oxygen (P1) (in table) of the **e** 3G18 and **f** 15G18 films

Table 4 Element concentration as calculated from the XPS spectra

Sample name	Element concentration (%)			
	Zn	O	Al	In
3G18	37.73	60	1.31	0.96
15G18	32.42	65.57	0.80	0.86

The variation of the electrical parameters such as resistivity (ρ), sheet resistance (R_s), carrier concentration (n_e), and Hall mobility (μ) with deposition pressures are shown in Table 5. It has been observed that resistivity values decrease with a decrease in the O_2 pressure. The values of carrier concentration and mobility increases with a decrease in the deposition pressure which is may be due to the enhancement in the V_O as supported by the XPS results. The carrier mean free path (L) has been evaluated using the following formula [48]:

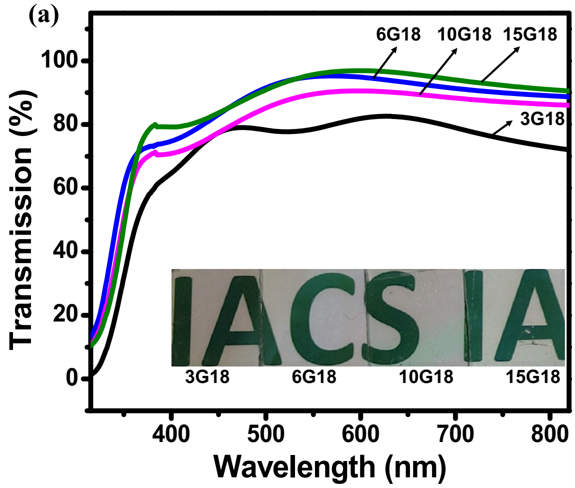

(b)

Sample name	Band-gap (eV)
3G18	3.68
6G18	3.62
10G18	3.60
15G18	3.55

Fig. 5 **a** Transmission spectra of the AIZO films. The inset shows the digital image of the write-up 'IACS' through the films. **b** Table shows the optical band-gap values of the AIZO films deposited at 180 mJ

Table 5 Resistivity, carrier concentration, sheet resistance, mobility, mean free path and FOM values of the various AIZO films

Sample name	Resistivity (Ω.cm)	Carrier concentration (cm^{-3})	Sheet resistance (Ω/sq)	Mobility (cm^2/V.s)	Mean free path (nm)	FOM (Ω^{-1})
3G18	1.10×10^{-3}	1.60×10^{21}	30.47	3.55	0.85	3.20×10^{-3}
6G18	1.24×10^{-3}	1.44×10^{21}	88.79	3.49	0.80	4.48×10^{-3}
10G18	2.38×10^{-3}	1.40×10^{21}	169.71	1.87	0.43	1.35×10^{-3}
15G18	4.77×10^{-3}	7.40×10^{20}	298.20	1.77	0.32	1.53×10^{-3}

$$L = \frac{h}{2e}\left(\frac{3n_e}{\Pi}\right)^{(1/3)}\mu \quad (4)$$

Where h is the Planck's constant and e the charge of the electron and the other symbols have been identified earlier. It has been observed that the mean free path value decreases as the pressure increases (Table 5), which indicates an enhancement in the scattering centers with an increase in the deposition pressure. Since the carrier concentration is high enough (> 5×10^{20} cm^{-3}) the contribution of grain boundary scattering can be neglected. However, Ghosh et al. [52] have shown that the boundary (BND) scattering plays a crucial role in controlling the mobility values for AZO films with the carrier concentration values in the order of 10^{21} cm^{-3}. Besides, the formation of oxygen interstitials (O_i) related acceptor-like complexes (such as D_{Zn}–O_i, D stands for dopant) maybe increased with increase in the deposition pressure, which limits the conductivity of the AIZO films deposited at higher deposition pressure [53].

Considering good crystallinity and high optical transparency we have chosen 180 mJ energy to deposit film on flexible PET substrate at 3×10^{-3} -mbar pressure.

The (002) peak at 2θ = 33.97^0 in the XRD pattern of the 3P18 film as shown in Fig. 6a confirms the crystallinity of the film just like the 3G18 film. Though the FWHM value is higher for the 3P18 film than the 3G18 film which indicates poor crystallinity for the 3P18 film.

The 3D AFM image in Fig. 6c shows the surface morphology of the 3P18 film. The calculated RMS roughness value is 1.6 nm for the 3P18 film. It has been observed from Fig. 6b that the film 3P18 shows almost similar transparency as compared to the 3G18 film. The bandgap value of the 3P18 has been calculated by Tauc plot and the value obtained is 3.69 eV which is almost same as that of the 3G18.

Figure 7 shows the comparison of Hall measurement data of the 3P18 film and commercial ITO-coated PET film. It has been observed that the 3P18 film shows very high carrier concentration of 1.87×10^{21} cm^{-3}, while the resistivity value is almost similar to that of the 3G18 film. The mobility value of the 3P18 is slightly lower than that of the 3G18 film.

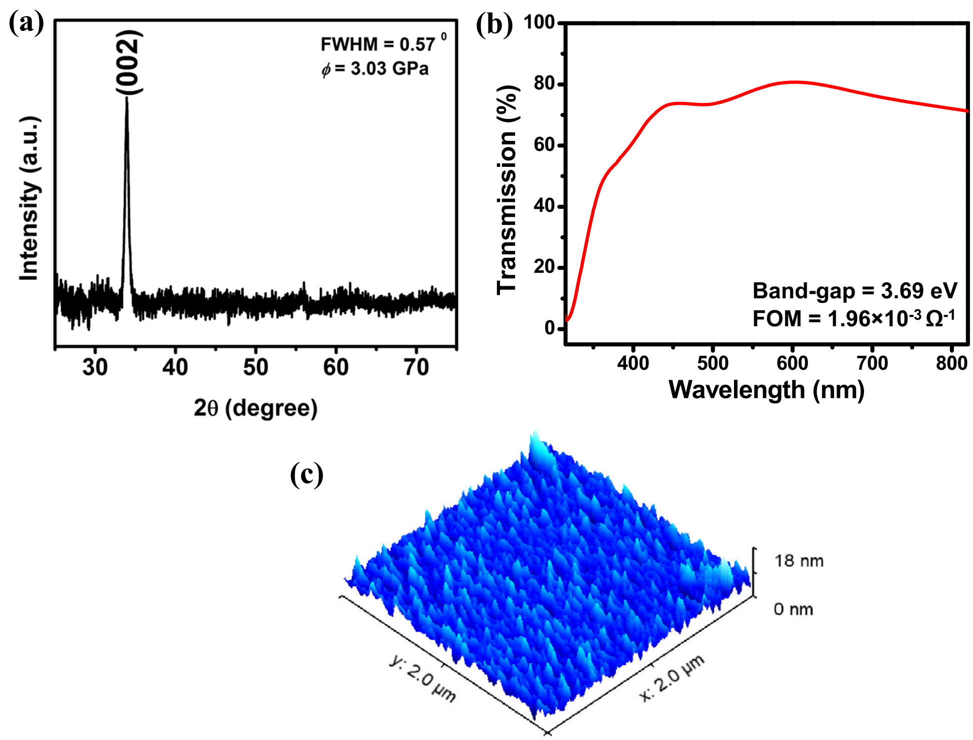

Fig. 6 **a** XRD pattern of the 3P18 film with FWHM value, compressive stress (ϕ) value of the corresponding film. **b** Transmission spectra of the 3P18 film with bandgap and FOM value of the corresponding film. **c** AFM image of the 3P18 film

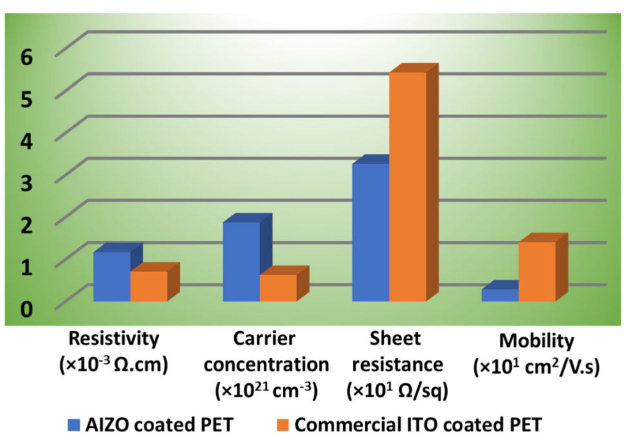

Fig. 7 Comparison of the resistivity, carrier concentration, sheet resistance, and mobility values of the AIZO-coated PET and commercial ITO-coated PET (Sigma-Aldrich) films

The sheet resistance of the 3P18 of value 32.63 Ω/sq is unexpectedly low which is highly suitable as TCF material. The FOM value of the 3P18 as obtained is $1.96 \times 10^{-3}\ \Omega^{-1}$, whereas the FOM for commercially available ITO-coated PET of Sigma-Aldrich [26] is $1.39 \times 10^{-3}\ \Omega^{-1}$, and Zhuhai manufactures [54] ITO-coated PET of FOM value ranging from 1.92×10^{-3} to $3.06 \times 10^{-3}\ \Omega^{-1}$.

Table 6 compares the doping element, doping percentage, deposition temperature, film thickness and sheet resistance of reported ZnO-based TCFs on PET substrates deposited by various techniques with those of our AIZO TCF on PET. It shows that our flexible TCF shows the lowest sheet resistance even when it is compared with the films deposited at temperatures higher than RT.

Resistance value of the 3P18 film with silver paste contacts using a multimeter in the bending condition has also been measured as shown in Fig. 8a which shows almost similar value as measured in the flat condition as shown in Fig. 8b.

4 Conclusion

In conclusion, AIZO thin films deposited by PLD technique at RT with an O_2 pressure of 3×10^{-3} mbar on PET substrate with a RMS roughness of 1.6 nm show very low sheet resistance of 32.63 Ω/sq. The experimental results clearly show that the AIZO film deposited on PET substrate makes it suitable for flexible TCF applications. This study is also helpful to understand the mechanism of co-doping in ZnO-based TCFs. These results are pertinent to the development of flexible electronics at low cost.

Table 6 Comparison of the deposition technique, doping element, doping percentage, deposition temperature, film thickness and sheet resistance values of some reported doped ZnO-coated PET TCFs

Deposition technique	Doping element	Doping percentage	Deposition temperature	Film thickness (nm)	Sheet resistance (KΩ/sq)	Ref
Atomic layer deposition	Al	–	100 °C	100	0.31	[55]
DC sputtering	Al	2 wt.%	RT	–	0.20–0.60	[56]
RF magnetron sputtering	Ga	5 wt.%	RT	150	0.23–53	[57]
RF magnetron sputtering	Al and Ga	0.32 wt.% and 0.18 wt.%	135 °C	100	37	[58]
PLD	Al and In	1 at.% and 1 at.%	RT	365	0.033	This work

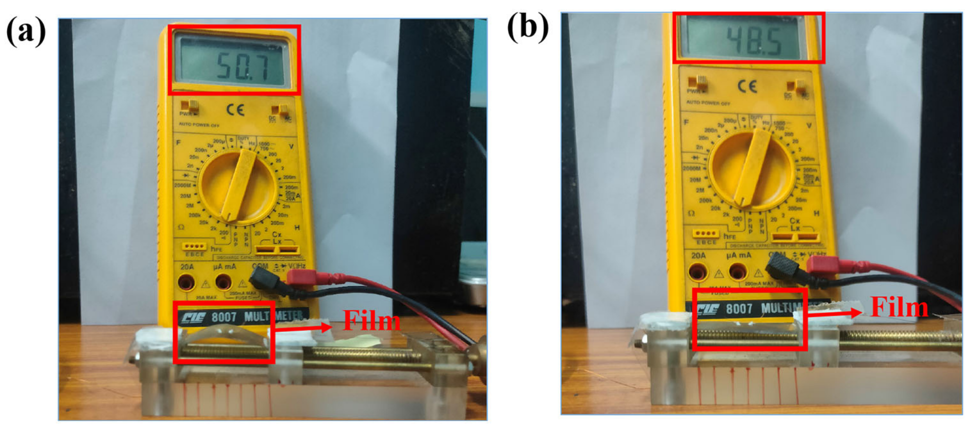

Fig. 8 Digital image with resistance value of the AIZO-coated PET substrate in the **a** bending and **b** flat conditions

Acknowledgements

One of the author S. Pal would like to thank DST-INSPIRE (IF190091), India for providing the fellowship.

Declarations

Conflict of interest The authors declare that they have no known competing financial interests or personal relationships that could have appeared to influence the work reported in this paper.

References

1. T. Minami, Transparent conducting oxide semiconductors for transparent electrodes. Semicond. Sci. Technol. **20**, S35–S44 (2005)
2. G.S. Chae, A modified transparent conducting oxide for flat panel displays only. Jpn. J. Appl. Phys. Part 1 Regul Pap. Short Notes Rev. Pap. **40**, 1282–1286 (2001)
3. B.G. Lewis, D.C. Paine, Applications and processing of transparent conducting oxides. MRS Bull. **25**, 22–27 (2000)
4. J.K. Sheu, Y.S. Lu, M.L. Lee, W.C. Lai, C.H. Kuo, C.J. Tun, Enhanced efficiency of GaN-based light-emitting diodes with periodic textured Ga-doped ZnO transparent contact layer. Appl. Phys. Lett. **90**, 3 (2007)
5. A. Tsukazaki, A. Ohtomo, T. Onuma, M. Ohtani, T. Makino, M. Sumiya, K. Ohtani, S.F. Chichibu, S. Fuke, Y. Segawa, H. Ohno, H. Koinuma, M. Kawasaki, Repeated temperature modulation epitaxy for p-type doping and light-emitting diode based on ZnO. Nat. Mater. **4**, 42–46 (2005)
6. J.K. Jha, R. Santos-Ortiz, J.C. Du, N.D. Shepherd, Semiconductor to metal transition in degenerate ZnO: Al films and the impact on its carrier scattering mechanisms and bandgap for OLED applications. J. Mater. Sci.-Mater. Electron. **25**, 1492–1498 (2014)
7. H.W. Lu, P.C. Kao, S.Y. Chu, Effects of ultra-thin al2o3-doped zno film as anode buffer layer grown by thermal evaporation for organic light-emitting diodes. ECS J. Solid State Sci. Technol. **6**, R14–R19 (2017)

8. A. Kim, Y. Won, K. Woo, C.H. Kim, J. Moon, Highly transparent low resistance ZnO/Ag nanowire/ZnO composite electrode for thin film solar cells. ACS Nano **7**, 1081–1091 (2013)
9. Y. Sobajima, S. Kato, T. Matsuura, T. Toyama, H. Okamoto, Study of the light-trapping effects of textured ZnO: Al/glass structure TCO for improving photocurrent of a-Si: H solar cells. J. Mater. Sci.-Mater. Electron. **18**, S159–S162 (2007)
10. D.C. Reyes, J.A. Mendez-Gamboa, M.R. Vidal, M. Acosta, Room-temperature ITO electrodes evaluated for organic solar cells using a photonic flux density figure of merit. J. Mater. Sci.-Mater. Electron. **29**, 11059–11064 (2018)
11. N.R. Armstrong, P.A. Veneman, E. Ratcliff, D. Placencia, M. Brumbach, Oxide contacts in organic photovoltaics: characterization and control of near-surface composition in indium-tin oxide (ITO) electrodes. Acc. Chem. Res. **42**, 1748–1757 (2009)
12. B. Yoo, K.J. Kim, D.K. Lee, K. Kim, M.J. Ko, Y.H. Kim, W.M. Kim, N.G. Park, Method to Protect Charge Recombination in the Back-Contact Dye-Sensitized Solar Cell. Opt. Express **18**, A395–A402 (2010)
13. W. Wei, V. Bhosle, C.M. Jin, R.J. Narayan, Optical and electrical properties of gallium-doped Mg15Zn85O thin films, in: J. Christen, C. Jagadish, D.C. Look, T. Yao, F. Bertram (Eds.) Zinc Oxide and Related Materials, Materials Research Soc, Warrendale, 2007, pp. 411
14. R. Meerheim, R. Nitsche, K. Leo, High-efficiency monochrome organic light emitting diodes employing enhanced microcavities. Appl. Phys. Lett. **93**, 3 (2008)
15. L.B. Duan, X.R. Zhao, J.M. Liu, W.C. Geng, C.D. Cao, M.M. Cao, Transparent and electrical properties of Ga-doped Zn1-x Cd (x) O films post-annealed in vacuum and nitrogen. J. Mater. Sci.-Mater. Electron. **24**, 2116–2121 (2013)
16. C. Lee, R.P. Dwivedi, W. Lee, C. Hong, W.I. Lee, H.W. Kim, IZO/Al/GZO multilayer films to replace ITO films. J. Mater. Sci.-Mater. Electron. **19**, 981–985 (2008)
17. B.P. Zhang, N.T. Binh, Y. Segawa, Y. Kashiwaba, K. Haga, Photoluminescence study of ZnO nanorods epitaxially grown on sapphire (11(2)over-bar0) substrates. Appl. Phys. Lett. **84**, 586–588 (2004)
18. L.C. Chen, C.A. Hsieh, X.Y. Zhang, Electrical Properties of CZO Films Prepared by Ultrasonic Spray Pyrolysis. Materials **7**, 7304–7313 (2014)
19. M. Sibinski, K. Znajdek, M. Sawczak, M. Gorski, AZO layers deposited by PLD method as flexible transparent emitter electrodes for solar cells. Microelectron. Eng. **127**, 57–60 (2014)
20. S. Ghosh, A. Mallick, B. Dou, M. Van Hest, S.M. Garner, D. Basak, A novel blanket annealing process to achieve highly transparent and conducting Al doped ZnO thin films: Its mechanism and application in perovskite solar cells. Sol. Energy **174**, 815–825 (2018)
21. K.U. Sim, S.W. Shin, A.V. Moholkar, J.H. Yun, J.H. Moon, J.H. Kim, Effects of dopant (Al, Ga, and In) on the characteristics of ZnO thin films prepared by RF magnetron sputtering system. Curr. Appl. Phys. **10**, S463–S467 (2010)
22. T. Minami, Substitution of transparent conducting oxide thin films for indium tin oxide transparent electrode applications. Thin Solid Films **516**, 1314–1321 (2008)
23. L.M. Wong, S.Y. Chiam, J.Q. Huang, S.J. Wang, J.S. Pan, W.K. Chim, Role of oxygen for highly conducting and transparent gallium-doped zinc oxide electrode deposited at room temperature. Appl. Phys. Lett. **98**, 3 (2011)
24. Y. Bin Xiao, S.M. Kong, E.H. Kim, C.W. Chung, Characteristics of indium zinc oxide thin films prepared by direct current magnetron sputtering for flexible solar cells. Sol. Energy Mater. Sol. Cells **95**, 264–269 (2011)
25. W.A. MacDonald, M.K. Looney, D. MacKerron, R. Eveson, R. Adam, K. Hashimoto, K. Rakos, Latest advances in substrates for flexible electronics. J. Soc. Inf. Disp. **15**, 1075–1083 (2007)
26. https://www.sigmaaldrich.com/catalog/product/aldrich/639303?lang=en&region=IN.
27. V. Kumar, R.G. Singh, L.P. Purohit, R.M. Mehra, Structural, transport and optical properties of boron-doped zinc oxide nanocrystalline. J. Mater. Sci. Technol. **27**, 481–488 (2011)
28. M.C. Jun, S.U. Park, J.H. Koh, Comparative studies of Al-doped ZnO and Ga-doped ZnO transparent conducting oxide thin films. Nanoscale Res. Lett. **7**, 6 (2012)
29. A. Mallick, D. Basak, Comparative investigation on cation-cation (Al-Sn) and cation-anion (Al-F) co-doping in RF sputtered ZnO thin films: Mechanistic insight. Appl. Surf. Sci. **410**, 540–546 (2017)
30. S. Ghosh, A. Mallick, A. Kole, P. Chaudhury, S. Garner, D. Basak, Study on AZO coated flexible glass as TCO substrate. in *2016 Ieee 43rd Photovoltaic Specialists Conference*. (IEEE, New York, 2016), pp. 634–638.
31. K. Yim, C. Lee, Dependence of the electrical and optical properties of sputter-deposited ZnO: Ga films on the annealing temperature, time, and atmosphere. J. Mater. Sci.-Mater. Electron. **18**, 385–390 (2007)
32. P. Mondal, S.K. Appani, D.S. Sutar, S.S. Major. (2021). Effect of oxygen partial pressure on the behavior of Ga-doped ZnO/p-Si heterojunction diodes fabricated by reactive sputtering, J. Mater. Sci.: Mater. Electron.
33. J.P. Kim, J.S. Bae, T.E. Hong, M.S. Won, J.H. Yoon, B.S. Lee, H.J. Lee, Optical and electrical properties of ZnO films, codoped with Al and Ga deposited at room temperature by an RF sputtering method. Thin Solid Films **518**, 6179–6183 (2010)

34. N. Martin, T. Nyberg, V. Kapaklis, Low temperature electronic transport in sputter deposited a-IGZO films. Curr. Appl. Phys. **14**, 1481–1485 (2014)
35. L. Zhang, J. Huang, J. Yang, K. Tang, B. Ren, Y. Hu, L. Wang, L.J. Wang, The effects of thickness on properties of B and Ga co-doped ZnO films grown by magnetron sputtering. Mater. Sci. Semicond. Process **42**, 277–282 (2016)
36. S. Dias, S. Chirakkara, N. Patel, S.B. Krupanidhi, Gallium and indium co-doped ZnO as a transparent conducting oxide for Cu2SnS3 photodetectors. J. Mater. Sci.-Mater. Electron. **29**, 2131–2139 (2018)
37. C.A. Gupta, S. Mangal, U.P. Singh, Impact of sputtering power on the properties of Al and Ga co-sputtered ZnO thin films. J. Mater. Sci.-Mater. Electron. **26**, 4280–4284 (2015)
38. A. Mallick, D. Basak, Revisiting the electrical and optical transmission properties Zok tor of co-doped ZnO thin films as n-type TCOs. Prog. Mater. Sci. **96**, 86–110 (2018)
39. H.U. Krebs, M. Weisheit, J. Faupel, E. Suske, T. Scharf, C. Fuhse, M. Stormer, K. Sturm, M. Seibt, H. Kijewski, D. Nelke, E. Panchenko, M. Buback, Pulsed laser deposition (PLD) - A versatile thin film technique, in *Advances in Solid State Physics 43*. ed. by B. Kramer (Springer-Verlag, Berlin, Berlin, 2003), pp. 505–517
40. R. Kumar, G. Kumar, A. Umar, Pulse laser deposited nanostructured ZnO thin films: a review. J. Nanosci. Nanotechnol. **14**, 1911–1930 (2014)
41. A. Mallick, S. Ghosh, D. Basak, Highly conducting and transparent low-E window films with high figure of merit values based on RF sputtered Al and In co-doped ZnO. Mater. Sci. Semicond. Process **119**, 10 (2020)
42. S. Mandal, A. Pandey, V.K. Komarala, Investigation of optoelectrical properties of indium oxide thin films with hydrogen and oxygen gas concentration variation during sputtering. Mater. Sci. Semicond. Process **123**, 9 (2021)
43. P. Murkute, H. Ghadi, S. Saha, S.K. Pandey, S. Chakrabarti, Enhancement in optical characteristics of c-axis-oriented radio frequency-sputtered ZnO thin films through growth ambient and annealing temperature optimization. Mater. Sci. Semicond. Process **66**, 1–8 (2017)
44. A. Das, G. Das, D. Kabiraj, D. Basak, High conductivity along with high visible light transparency in Al implanted sol-gel ZnO thin film with an elevated figure of merit value as a transparent conducting layer. J. Alloy. Compd. **835**, 11 (2020)
45. Z.G. Zhang, F. Zhou, X.Q. Wei, M. Liu, G. Sun, C.S. Chen, C.S. Xue, H.Z. Zhuang, B.Y. Man, Effects of oxygen pressures on pulsed laser deposition of ZnO films. Phys. E. **39**, 253–257 (2007)
46. S.S. Kim, B.T. Lee, Effects of oxygen pressure on the growth of pulsed laser deposited ZnO films on Si(001). Thin Solid Films **446**, 307–312 (2004)
47. M.N. Islam, T.B. Ghosh, K.L. Chopra, H.N. Acharya, XPS and X-ray diffraction studies of aluminum-doped zinc oxide transparent conducting films. Thin Solid Films **280**, 20–25 (1996)
48. Y.Q. Wang, W. Tang, L. Zhang, Crystalline Size Effects on Texture Coefficient, Electrical and Optical Properties of Sputter-deposited Ga-doped ZnO Thin Films. J. Mater. Sci. Technol. **31**, 175–181 (2015)
49. S. Rahmane, M.A. Djouadi, Optoelectronic properties of ZnO thin films grown by radio frequency magnetron sputtering. J. Mater. Sci.-Mater. Electron. **31**, 17872–17878 (2020)
50. Y. Wu, F. Cao, X.H. Ji, Optical and electrical properties of Al-doped ZnO thin films by atomic layer deposition. J. Mater. Sci.-Mater. Electron. **31**, 17365–17374 (2020)
51. T. Minami, T. Miyata, R. Uozaki, H. Sai, T. Koida, Textured surface structures formed using new techniques on transparent conducting Al-doped zinc oxide films prepared by magnetron sputtering. Thin Solid Films **614**, 56–61 (2016)
52. S. Ghosh, D. Basak, Correlation between hall mobility and optical mobility in aluminum-doped zno films via boundary scatterings and estimation of donor compensation ratio. Physica Status Solidi B **257**, 1900682 (2020)
53. J.T. Thienprasert, S. Rujirawat, W. Klysubun, J.N. Duenow, T.J. Coutts, S.B. Zhang, D.C. Look, S. Limpijumnong, Compensation in Al-Doped ZnO by Al-Related Acceptor Complexes: Synchrotron X-Ray Absorption Spectroscopy and Theory. Phys. Rev. Lett. **110**, 5 (2013)
54. http://www.zh-kv.com/Kaivo_En/ProductView.asp?ID=19&SortID=128.
55. D. Dimitrov, C.L. Tsai, S. Petrov, V. Marinova, D. Petrova, B. Napoleonov, B. Blagoev, V. Strijkova, K.Y. Hsu, S.H. Lin, atomic layer-deposited Al-doped ZnO thin films for display applications. Coatings **10**, 11 (2020)
56. Z.L. Pei, X.B. Zhang, G.P. Zhang, J. Gong, C. Sun, R.F. Huang, L.S. Wen, Transparent conductive ZnO: Al thin films deposited on flexible substrates prepared by direct current magnetron sputtering. Thin Solid Films **497**, 20–23 (2006)
57. B.G. Kim, J.Y. Kim, S.J. Lee, J.H. Park, D.G. Lim, M.G. Park, Structural, electrical and optical properties of Ga-doped ZnO films on PET substrate. Appl. Surf. Sci. **257**, 1063–1067 (2010)
58. C.Y. Tsay, K.C. Pai, Properties of Al-Ga co-doped ZnO semiconductor thin films deposited on polyethylene terephthalate substrates by radio frequency magnetron sputtering. Thin Solid Films **654**, 11–15 (2018)